Growth and optimization of 2 μm InGaSb/AlGaSb quantum well based VECSELs on GaAs/AlGaAs DBRs.

Pankaj Ahirwar, Thomas J. Rotter, Darryl Shima, Nahid A. Jahan, Stephen P. R. Clark, Sadhvikas J. Addamane, Ganesh Balakrishnan, Senior Member, *IEEE*, Alexandre Laurain, Jörg Hader, Yi-Ying Lai, Jerome V. Maloney, Ikuo Suemune, R. Bedford

***Abstract*— We report the growth of optically pumped vertical external cavity surface emitting lasers (VECSELs) based on InGaSb/AlGaSb quantum wells grown on GaAs/AlGaAs distributed Bragg reflectors (DBRs), which are in turn grown on GaAs substrates. We attempt to mitigate the effects of the 7.78% lattice mismatch that exists between GaSb and GaAs by introducing an interfacial layer of 90º misfit dislocations (IMF) at the mismatched interface. This results in the spontaneous relaxation of the GaSb epi-layer and significantly reduces threading dislocation density. The IMF interface is optimized through the use of an antimony soak layer, which results in a distinct (2 x 8) Sb reconstructed surface on GaAs. The III-Sb VECSEL active region is optimized for various parameters including quantum well quality and the thickness of the individual layers. The VECSELs are optically pumped using both pulsed sources for sub-thermal measurements and continuous wave (CW) sources. The pulsed measurements have resulted in record results of 340 W peak power while the CW measurements have resulted in a maximum output power of 0.12 W, with both lasers emitting at 2 μm. We investigate the effects of the mismatched interface by comparing the III-Sb VECSEL grown on GaAs/AlGaAs DBRs to a lattice matched III-Sb VECSEL grown on GaSb/AlAsSb DBRs. The results indicate deterioration in the lattice-mismatched laser's performance compared to the lattice-matched laser's performance in terms of threshold pump density, efficiency and maximum CW output power. Further comparison of the structures using cross-section transmission electron microscopy also confirms the presence of threading dislocations in the III-Sb active region grown on GaAs/AlGaAs DBRs. The ability to use such mismatched active regions will therefore depend on the stability and reproducibility of the IMF interface. The optical properties of the III-SB active regions grown on the GaAs substrates using IMF technique are investigated using time-resolved photoluminescence with the objective of using this technique to optimize the IMF interface in future studies.**

***Index Terms*— Semiconductor lasers, Quantum well lasers, Surface-emitting lasers.**

I. Introduction

The two-micron vertical external cavity surface emitting laser has applications in a variety of technologies from gas sensing to infrared counter measures. The use of antimonide semiconductors for lasers in the 1.8 – 3.3 μm wavelength range is well established with a majority of such lasers fabricated as edge emitting diodes including distributed feed-back (DFB) lasers. [1] However, the high beam quality and high output power of the VECSEL could be of considerable advantage to the antimonide lasers in this wavelength range.

The power scaling in a VECSEL is achieved by increasing the diameter of the pump spot while keeping the pump density constant. The quantum well VECSELs based on InGaAs quantum wells grown on GaAs substrates have recently broken the 100 Watt barriers for CW output power from a single chip. [2] However, the same level of success has not been achieved with antimonide VECSELs, which are yet to reach 10 Watts CW. The main reason for the "order of magnitude" reduction in the maximum CW power achieved by VECSELs on GaAs versus the GaSb based lasers can be attributed to thermal management issues. The InGaAs based lasers are based on a mature substrate removal technology that permits the complete substrate removal and the ability to bond the laser extra-cavity to CVD diamond. The lack of such an etch stop layer in antimonides have restricted these lasers to thermal management schemes that require intra-cavity heat spreading. The use of intra-cavity heat spreaders such as transparent diamond invariably leads to interaction of the stimulated photons in the cavity with defects in the diamond and this source of loss is significant enough to restrict the performance of the lasers. Thus, the ability to grow antimonide VECSELs on a substrate with an established etch stop recipe such as on GaAs or InP could lead to significant improvements in the thermal management of the antimonide

Manuscript received November 1, 2012. This research was conducted at the University of New Mexico and was funded by the following grants: USAFOSR Grant Nos. FA9550-09-1-0202, FA9550-07-1-0573 and DoD HBCU/MI grant W911NF-12-1-0058.

Pankaj Ahirwar, Thomas J. Rotter, Darryl Shima, Stephen P. R. Clark, Sadhvikas Addamane, Ganesh Balakrishnan are with the Center for High Technology Materials at the University of New Mexico, Albuquerque, NM 87106, USA (e-mail: panki@chtm.unm.edu, tjr@chtm.unm.edu, dmshima@unm.edu, zippyz2@unm.edu, addamane@unm.edu, gunny@unm.edu).

Alexandre Laurain, Jörg Hader, Yi-Ying Lai and Jerome V. Maloney are with the College of Optical Sciences, University of Arizona, Tucson, AZ 85721, USA (e-mail: alaurain@email.arizona.edu, jhader@acms.arizona.edu, yylai@acms.arizona.edu, jml@acms.arizona.edu).

Nahid A. Jahan and Ikuo Suemune are with the Research Institute for Electronic Science, Hokkaido University, Sapporo, 001-0021, Japan (e-mail: nahidajahan@yahoo.com, isuemune@es.hokudai.ac.jp).

R. Bedford is with the Air Force Research Laboratory, Wright Patterson AFB, Ohio 45433, USA (Robert.Bedford@wpafb.af.mil).

lasers and consequently a much higher value for the maximum CW output power from the lasers.

One such strategy to achieve antimonide VECSELs on GaAs would be develop the growth of antimonide active regions on GaAs substrates which would allow for complete substrate removal without the need for an etch stop layer. A citric acid based etch has a high selectivity between GaSb and GaAs and can thus result in complete removal of the substrate. However the main issue with this approach is the 7.78% mismatch that exists between the GaSb and the GaAs binaries, which could lead to extensive threading dislocations in the GaSb epilayer and hence result in significant non-radiative recombination losses in the antimonide active region. Furthermore, if the growth of the antimonide active region is done on a GaAs substrate, the first quantum well is typically within 500 nm of the mismatched interface. Thus, apart from the issue of excessive threading dislocations we must also address the issue of non-reproducible relaxation in the antimonide buffer. If the antimonide buffer does not relax reproducibly, then the in-plane lattice constant of the buffer will change from run to run, which would also change the strain in the quantum wells from run to run. Such issues lead to performance degradation in edge-emitters, however in a vertical cavity laser where the position of the gain-peak and the micro-cavity resonance need to be precise, a variation in the gain peak could be significantly more catastrophic. Thus any metamorphic buffer based approach has to result in two conditions in the active region – a) the antimonide layer should have the minimum possible threading dislocation density and b) the buffer must have a highly reproducible lattice constant with preferably a 100% relaxation.

In this body of research we explore the ability to grow GaSb based active regions directly on GaAs substrates by inducing an interfacial array of misfit dislocations. The study further investigates the ability to grow such active regions on GaAs/AlGaAs DBR to investigate the effects of the highly mismatched interface on the performance of the laser. Finally, we shall conduct cross-section transmission electron microscopy investigation of the VECSEL structures.

II. Epitaxial growth of the VECSELs.

A VECSEL typically consists of a semiconductor gain mirror and an external mirror (also known as output coupler). The optical mode in the device forms a standing wave pattern between the two mirrors. The gain-medium (QW) needs to be placed at the antinodes of the standing E-field for optimum device performance. [3,4] This design is usually referred to as a Resonant Periodic Gain (RPG) structure. The distance between the QW layers corresponds to an optical path length of $\lambda/2$, with 9 QWs the total length of the III-Sb sub-cavity roughly corresponds to a thickness of ~ 5λ. The sub-cavity length also plays an important role in the pump absorption. The incident pump radiation is absorbed both by barriers and wells; however, the well thickness in the design is 1/20 times that of barrier, therefore multiple QWs are required for lasing of the VECSEL device. Due to low gain from the thin QW active-region, a high reflectivity **R ~ 99%** is needed to achieve lasing. [1] This is achieved using a high reflectivity mirror (DBR), which consists of $\lambda/4$ optical thickness layers of alternating high ($\mathbf{n_H}$) and low ($\mathbf{n_L}$) index of refraction. The DBR reflectivity ($\mathbf{R_{DBR}}$) depends on the index contrast ($\mathbf{n_H}$-$\mathbf{n_L}$) and the number of DBR periods.

The VECSEL devices discussed in this paper comprise of a III-Sb based active region emitting at or near 2 μm grown epitaxially on GaAs/AlGaAs DBRs and also grown lattice matched to GaSb/AlAsSb DBRs for comparison. The gain is provided by 9 QWs, each 13 nm wide $Ga_{0.8}In_{0.2}Sb$ separated by 260.4 nm $Al_{0.25}Ga_{0.75}Sb$ barriers. The active-region and AlAsSb/GaSb DBR is epitaxially grown by elemental source molecular beam epitaxy in a VG Semicon V80H reactor and in the case of the antimonide VECSEL on GaAs/AlGaAs DBRs the active region is MBE grown and the DBR is MOCVD grown. In case of the all-antimonide VECSEL, the entire structure is lattice matched to the GaSb substrate while in the case of the antimonide VECSEL on GaAs/AlGaAs, the active region has a lattice constant of 6.09 Å while the DBR is lattice matched to GaAs. In this section we shall discuss the designs of the all-antimonide lattice matched VECSEL and compare it to a design for an antimonide active region based VECSEL on a GaAs/AlGaAs DBR. We shall also discuss the growth strategies used to achieve an interfacial array of misfit dislocation at the GaSb/GaAs interface.

A. 2 μm VECSEL structure on GaAs/AlGaAs DBRs.

Figure 1(a) shows a schematic illustration of the fabricated VECSEL structure on a GaSb substrate. The bottom DBR is comprised of 19 pairs of $AlAs_{0.08}Sb_{0.92}$ (153.8 nm) / GaSb (132.6 nm). The active-region consists of 9 $In_{0.2}Ga_{0.8}Sb$ QW separated by pump absorbing $Al_{0.25}Ga_{0.75}Sb$ barriers. An AlSb confinement layer on each side of the active region ensures carrier confinement in the structure, and a thin GaSb capping layer is added on top to prevent oxidation. A low-resolution TEM image of the structure is shown in Figure 1(b), the structure matches the epitaxially grown structure (only a few DBR-pairs are captured in image). Figure 1(c) shows E-field and refractive index profile for the lattice-matched VECSEL.

The schematic illustration and low-resolution TEM image of the VECSEL structure grown on a GaAs substrate is shown in Figures 2(a) and 2(b) respectively. Figure 2(c) shows E-field and refractive index profile for the lattice-mismatched VECSEL. The bottom DBR in this device consists of 25 pairs of $Al_{0.95}Ga_{0.05}As$ (172 nm)/GaAs (149 nm) which is grown using metal–organic chemical vapor deposition (MOCVD). The active region is then grown by MBE. It also consists of 9 $In_{0.2}Ga_{0.8}Sb$ QW separated by pump absorbing $Al_{0.25}Ga_{0.75}Sb$ barriers and AlSb top/bottom-clad.

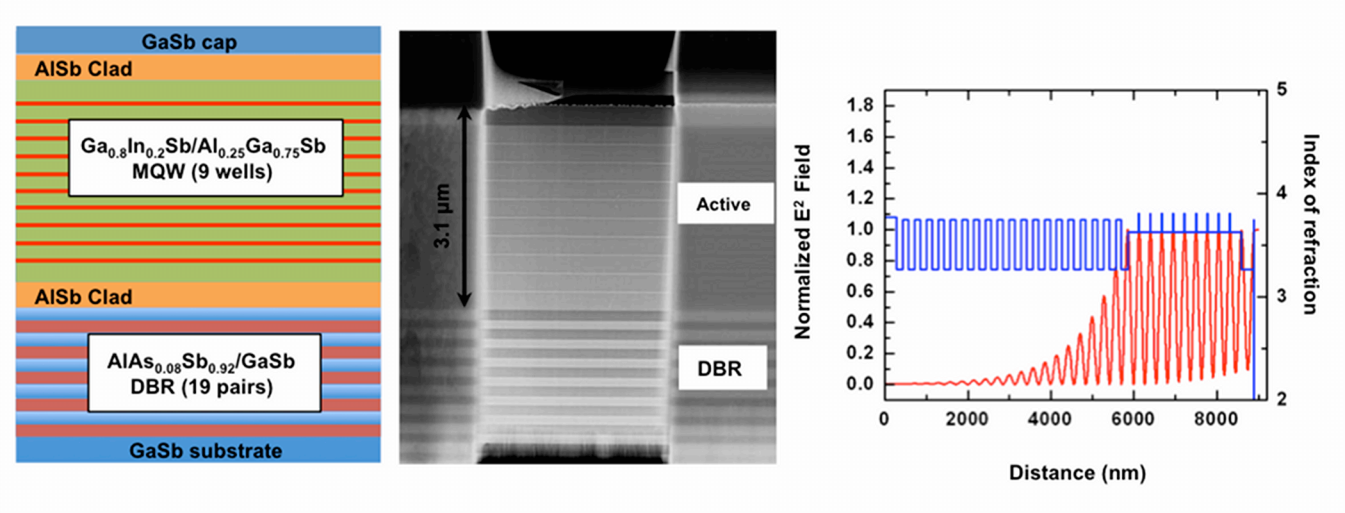

Figure 1: Schematic, cross-section TEM image and plot of refractive index and E-field for lattice-matched 2µm III-Sb VECSEL grown on GaSb/AlAsSb DBR.

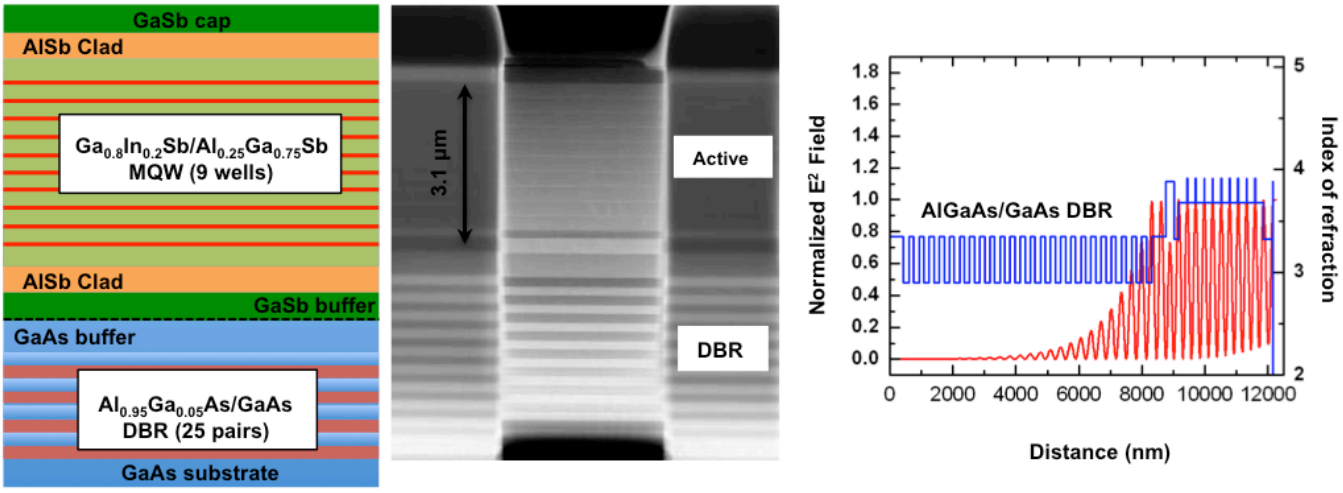

Figure 2: Schematic, cross-section TEM image and plot of refractive index and E-field for lattice-mismatched 2µm III-Sb VECSEL grown on GaAs/AlGaAs DBR.

The key feature of the antimonide VECSEL based on the GaAs/AlGaAs DBRs is the ability to achieve lasing despite the 7.78% mismatched interface between the antimonide active region and the arsenide based DBR. The first quantum well is located within 500 nm of this highly mismatched interface. Thus for such a VECSEL to work the growth has to be optimized to achieve minimal threading dislocations in the active region and to achieve a reproducible relaxation of the metamorphic buffer.

B. Interfacial misfit dislocation array based growth of GaSb on GaAs.

The growth of the antimonide active regions on GaAs/AlGaAs distributed Bragg reflectors is based on an interfacial layer of 90º misfit dislocations at the GaSb/GaAs growth interface. A key requirement for the VECSEL structure is to achieve large areas of periodically spaced misfit dislocations so that the GaSb epi layer spontaneously relaxes and has low threading dislocation density. As is shown in Figure 2(a), (b), the first quantum well in the laser design is located ~ 400 nm from the 7.8% mismatched interface. Threading dislocations would introduce a strong non-radiative recombination process and relaxation that is not 100% would make the strain in the quantum wells unpredictable.

Researchers such as Rocher et. al. [5] have shown that such periodic misfit dislocation arrays exist beneath GaSb islands grown on GaAs substrates. These are 90 º misfit dislocations

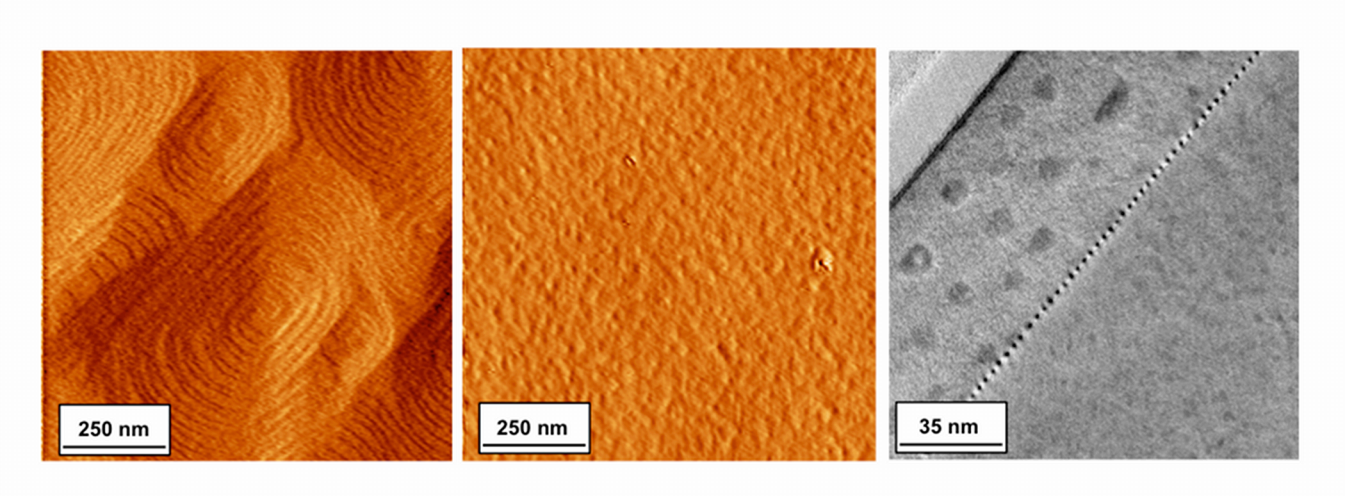

Figure 3: (a) Atomic force micrograph of GaSb on GaAs without the formation of the IMF array. (b) Atomic force micrograph of GaSb on GaAs with an optimized IMF array at the GaSb/GaAs interface. (c) cross-section TEM image of GaSb grown on GaAs with a periodic IMF array at the interface.

arrays with the 56 Å periodicity corresponding to completely relaxed GaSb on GaAs. The growth of GaSb on GaAs is thus fundamentally different from the growth of a similarly mismatched alloys such as InAs on GaAs. While InAs tends to grow in a Stransky-Krastanov growth mode where the coherent strain in the epi-layer is relieved through the growth of 3-dimensional nano-structures to manage the strain, the growth of GaSb proceeds in a spontaneous relaxation regime with the islands achieving close to 100% relaxation within the first monolayer of growth. This periodic 90º-misfit dislocation array at the GaSb/GaAs interface is the primary mechanism for accommodating this mismatch. These periodic misfit dislocations spaced at ~ 56 Å along both the [110] and [1-10] directions correspond to 13 lattice sites of GaSb or 14 lattice sites of GaAs. The 13:14 ration between the GaSb and the GaAs lattice sites is the minimum value for the mismatch between the two lattice constants and can be interpreted as an energy minimization process that is achieved through self-assembly or packing of Sb atoms on a GaAs surface.

Kaspi et. al. [6] further identified and documented the fact that the threading dislocation density in the bulk growth of GaSb on GaAs comes from the coalescence of such islands. This is due to the fact that when two independent chains of periodic 90º dislocations merge, the periodicity of the misfit dislocations at the point of coalescence is lost. This leads to the formation of 60º-misfit dislocations that have a very high probability of threading into the epilayer. Therefore, the less the number of islands and the larger their size, the lower the threading dislocation density in the bulk GaSb. The growth of the GaSb mismatched epilayers on GaAs was also investigated by Brar et al. [7] who for the first time showed the presence of extensive screw dislocations in the epi-layer. These results were further investigated by Shanabrooke et al. [8] A typical non-IMF growth of GaSb on GaSb with screw dislocations is show in Figure 3(a).

Thus while the GaSb islands grown on GaAs are free of threading dislocations, the epilayer grown as a result of the coalescence of these islands has a threading dislocation density strongly correlated to the island density and more specifically to number of coalescence sites.

Thus to achieve low threading dislocation density of GaSb on GaAs either the number of coalescence sites have to be significantly reduced or the arrays of 90º misfit dislocations under all islands have to be linked to form a coherent series. One such method for the reduction of threading dislocations for GaSb on GaAs is to use an Sb (2 x 8) reconstruction on the GaAs surface prior to the growth of the GaSb epilayer. We have termed this reconstruction assisted interfacial misfit dislocation arrays. The reconstruction assisted interfacial misfit-dislocation array is a fundamentally unique epitaxial growth mode based on atomic self-assembly of group V ad-atoms at a lattice-mismatched interface. [9] The basic mechanism for the formation of such an interface is the realization of specific antimony surface reconstructions on the GaAs substrate. These are usually multi-layer reconstructions such as the (2 x 8) Sb reconstruction that surpasses the critical-thickness for the GaSb/GaAs material system without the actual growth of any GaSb. These multi-layer antimony reconstructions are completely strain-relieved and achieve this by forming the 90º misfit-dislocations at the Sb/GaAs interface. The misfit dislocations are spaced uniformly 56 Å apart. This 56 Å periodicity also corresponds to completely relaxed GaSb on GaAs since the spacing is equivalent to 13 lattice sites of GaSb or 14 of GaAs along the [110] direction and this can be shown to be the best possible ratio for relaxed GaSb on GaAs. [10] The AFM and cross-section TEM image of the IMF based growth of GaSb on GaAs is shown in Figures 3 (b) and (c) respectively. The AFM shows the complete elimination of screw dislocations while the TEM shows the IMF array and a low threading dislocation density GaSb layer on GaAs. The

reconstruction's ability to self-assemble and dynamically change its coverage on the substrate allows for a monolayer of completely relaxed GaSb to be realized across the GaAs substrate. At present, we have seen a network of such intact misfit dislocations across several square microns in area. In theory such a periodic array should exist across the GaAs substrate regardless of its diameter. However, steps in the wafer and Arsenic intermixing in the Sb reconstruction have restricted these dislocation arrays to a few square microns in area. A threading dislocation density of 5 x 10^6/cm^2 has been observed. [11] The reduction in threading dislocation density is further evidenced by the published device results from this technique. This growth method has been used to demonstrate novel lasers and detectors based on the integration of antimonide lasers with GaAs and Silicon substrates. [12,13]

C. *Optimization of IMF based Quantum wells*

The quantum well emission wavelength depends on the In content x and the thickness of the $Ga_{1-x}In_xSb$ quantum wells. At the typical growth temperatures (460 – 500°C), the re-evaporation of In from the substrate is not negligible, thus the actual In content of the quantum well material depends not only on the nominal In flux but also on the growth temperature. Furthermore, the quantum well's emission wavelength and strength depends on its strain. The optical quality of the quantum wells depends on their growth temperature. Finally the Sb flux supplied during growth of the active region becomes important with increasing III-Sb thickness. This also depends on the growth temperature. Thus the quantum wells have to be optimized with respect to nominal In content, thickness as well as growth temperature and Sb flux.

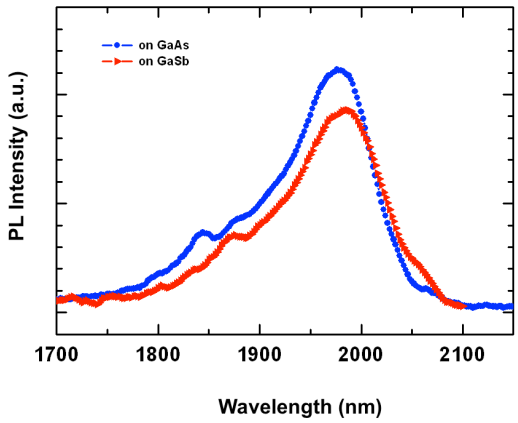

Figure (4) PL of a structure with 11 nm thick $Ga_{0.75}In_{0.25}Sb$ quantum wells, grown on a GaAs substrate (blue), and grown on a GaSb (red).

As optimization parameter the photoluminescence (PL) intensity is used, as it is a good measure for the material's optical quality, and therefore important for optical gain in a laser. Test samples with four quantum wells have been grown on GaAs, using the interfacial layer of 90° misfit dislocations. For comparison test structures have been grown directly on GaSb also. Figure 4 shows the PL of a sample with an 11nm thick $Ga_{0.75}In_{0.25}Sb$ well, grown on GaAs and on GaSb. The PL intensity from the sample grown on GaAs exceeds the one from the sample grown directly on GaSb by 20%, indicating, that the material's optical quality grown on GaAs is not significantly inferior to the material grown directly on GaSb. However, small differences in strain between antimonide layers grown on GaAs with the interfacial layer of 90° misfit dislocations compared to those grown on GaSb can influence the strain in the quantum wells. This influences the optical emission from the III-Sb active region, since it depends on the compressive strain in the quantum wells. Therefore the active region for growth on GaAs has to be developed independently from that for growth on GaSb.

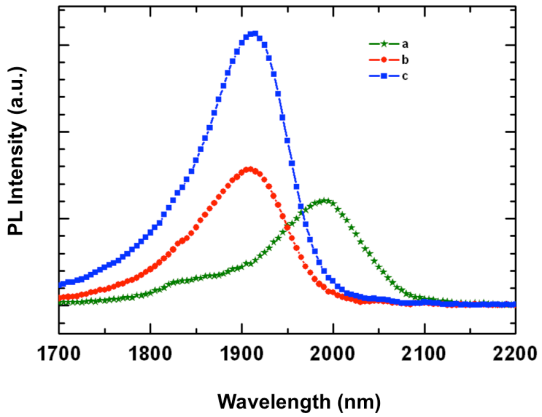

Figure (5) *PL of a structure with 10 nm thick $Ga_{0.72}In_{0.28}Sb$ quantum wells, grown at 475 °C (a), and at near 490 °C (b). For comparison the emission wavelength of b can also be achieved by a structure with 12 nm thick $Ga_{0.8}In_{0.2}Sb$ well, grown at 475 °C (c).*

The growth temperature is controlled in situ by surface pyrometry. Figure 5 shows the influence of the growth temperature. Samples *a* and *b* have nominally the same quantum wells (10 nm wide $Ga_{0.72}In_{0.28}Sb$), but are grown at different temperatures, 475 °C and near 490 °C, respectively. The emission wavelength of *b*, grown at higher temperature, is blue shifted by about 85 nm compared to *a*. The PL's peak intensity is about 30% higher. On the other hand, the shorter emission wavelength can also be achieved by growing a 12 nm thick $Ga_{0.8}In_{0.2}Sb$ well at 475 °C, sample *c*, yielding more than twice the peak PL power.

The optimal growth temperature of the quantum wells for an emission wavelength near 2 µm was determined to be 470°C. The layers grown before the first quantum well can be grown at higher temperature, e.g. 510°C for the III-Sb, and 580°C for the III-As. Beginning with the first quantum well and all following layers have to be grown at low temperature, since the GaInSb quantum wells deteriorate even if the temperature is increased only after they are already buried in AlGaSb. This is in difference to GaInAs QWs in III-As active regions.

For the VECSEL, the III-Sb layers have to be grown on the AlGaAs/GaAs DBR instead of on GaAs. The DBR exhibits a slightly higher surface roughness compared to a GaAs substrate. This is associated with the strain due to the Al. It results in surface features elongated along the [011] direction. The average surface roughness is 0.3nm RMS. The increased surface roughness likely limits the formation of the 90º-misfit dislocation array and potentially results in a higher density of threading dislocations compared to growth on smooth, epi ready GaAs substrates.

For the growth of the entire active region with 9 quantum wells, the optimization of the Sb flux during growth becomes important. The PL intensity increases by 17x when the Sb flux was reduced from 3 x 10^{-6} mbar to 1 x 10^{-6} mbar, see Figure 6 Generally, the PL intensity rises with lower Sb flux, until a minimum Sb flux, below which the substrate surface becomes group III rich and turns hazy. This minimum Sb flux depends on the growth temperature. The minimum Sb:Ga flux ratio is about 2.5 for growth temperatures near 470C.

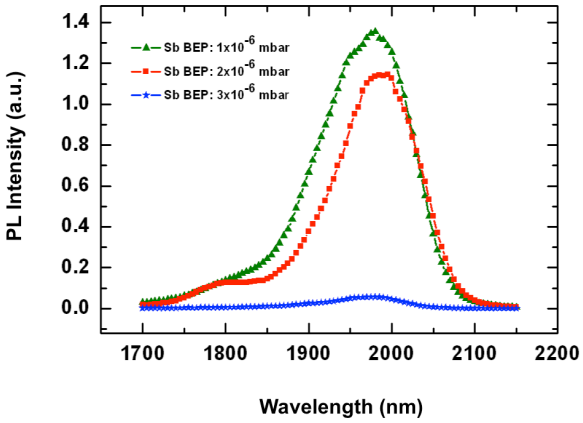

Figure (6) Influence of the Sb flux, measured as beam equivalent pressure (BEP) on the PL of a VECSEL active region with 9 quantum wells (grown on GaAs).

The PL optimization resulted in two quantum well designs, 10nm $Ga_{0.72}In_{0.26}Sb$ – quantum wells in $Al_{0.3}Ga_{0.7}Sb$ barriers and 13nm $Ga_{0.8}In_{0.2}Sb$ – quantum wells in $Al_{0.25}Ga_{0.75}Sb$ barriers. However, the latter design consistently led to superior laser performance.

D. VECSEL growth optimization

For optimized device performance it is essential to precisely place the QWs at E-field antinodes within the sub-cavity. This requires precise control of growth rates of the group-III sources of MBE, as growth rate variation can affect both composition and thickness of the constituent layers. The growth rates are calibrated using RHEED oscillations.

The quantum well gain region is characterized by its photoluminescence spectrum. The PL spectrum measured normal to the wafer surface is strongly modulated due to the sub cavity etalon and the DBR. The edge-PL spectrum shows significantly weaker modulation and is therefore used to determine the QW emission's spectral peak position [1,4,14]. The VECSEL sample is mounted on a heat sink to measure the edge/surface PL spectrum at different heat-sink temperatures. Figures 7 and 8 shows edge/surface PL spectra from a VECSEL sample. The edge-PL shifts to longer wavelength at about 1.6nm/K [14], this is primarily due to the bandgap energy temperature dependence. The sub cavity resonance also shifts to longer wavelength with increasing temperature, but more slowly when compared to

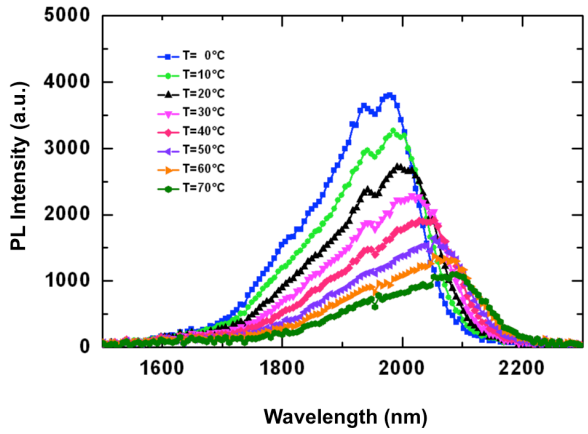

Figure 7: Edge PL spectra from a VECSEL sample.

intrinsic gain-peak shift; at about 0.26nm/K. The sub cavity resonance peak shift is due to temperature dependence of refractive indices. The determination of gain-peak and sub cavity resonance shift with respect to temperature is useful for proper design of the VECSEL. To achieve high CW output power the gain-peak emission is typically designed to be 30-50nm shorter than the actual desired wavelength of device operation, such that the gain-peak and sub cavity resonance coincide at the desired operating temperature. The operating temperature depends on heat-sink temperature and power dissipated in active region.

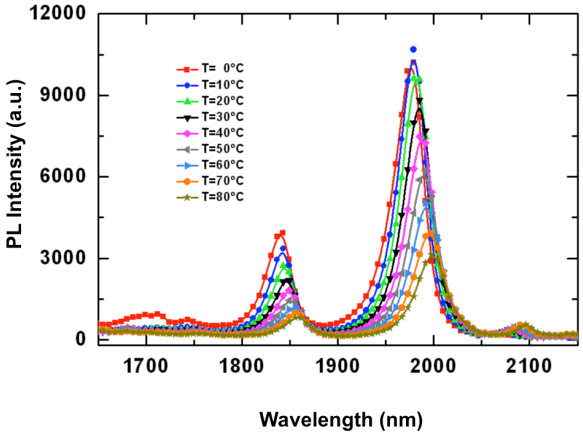

Figure 8: Surface PL spectra from a VECSEL sample.

The reflectivity spectrum is measured by a FTIR with the VECSEL chip mounted on a heat sink. Figure 9 shows the reflectivity spectrum at different heat-sink temperatures. The reflectivity spectrum shows the effect of the sub cavity etalon formed between DBR and air-semiconductor interface. The reflectivity spectrum is used to diagnose the deviation in thickness of layers and composition of both DBR and sub cavity. For the reflectivity spectrum in Figure 9 we observe that the most optimized overlap between intrinsic QW gain-peak and sub cavity resonance is at heat sink temperature of 70 ^{o}C. This indicates a good agreement between the design and the epitaxially grown VECSEL sample.

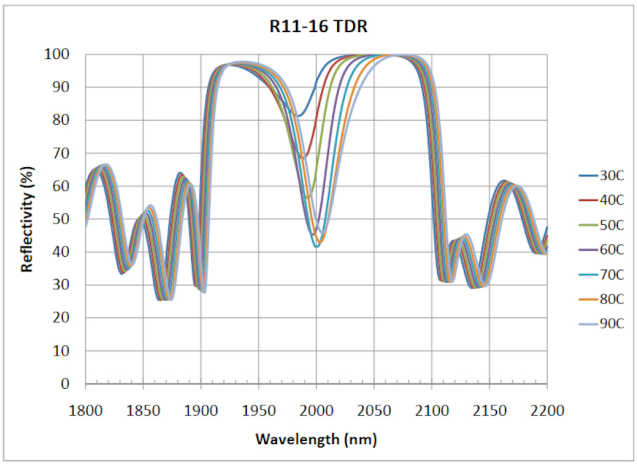

Figure 9: Temperature dependent reflectivity spectra from a VECSEL on GaAs/AlGaAs DBR.

III. LASER CHARACTERIZATION.

The VECSEL cavity is formed between DBR and an external output coupler. The output coupler radius of curvature (R_{OC}) and cavity length (L) is chosen to achieve optimal matching between optical mode and gain aperture size. The output coupler radius of curvature (**R_{OC}**) and cavity length (**L**) are related to gain-aperture size (**w**) for a linear cavity through following equation, [15]

$$w = \sqrt[4]{\frac{R_{OC}L\lambda^2 - L^2\lambda^2}{\pi^2}} \qquad (1)$$

where λ is the wavelength. The pump-spot size is adjusted to match the beam-waist size of the linear cavity as closely as possible by the two pump focussing lenses. For laser characterization of the VECSEL sample grown on GaAs, a linear cavity consisting of a curved output coupler (with **R_{OC}** = 70 - 100mm and **R** ~ 99%) is used.

Pulsed lasing characterization.

The VECSELs with III-Sb active regions and AlGaAs/GaAs DBRs were initially pumped optically by a pulsed source. This allows operation of the laser in a sub-thermal regime without heat spreading elements. Figure 10 shows the experimental setup. The pump-laser is a diode-pumped Nd:YAG laser. The repetition rate is 1kHz and pulse width τ_{pulse} ~ 300ns , with available peak-power up to 1.2 kW. The diameter of pump-spot is adjusted by varying the distance between the VECSEL-chip and the pump-focusing lens.

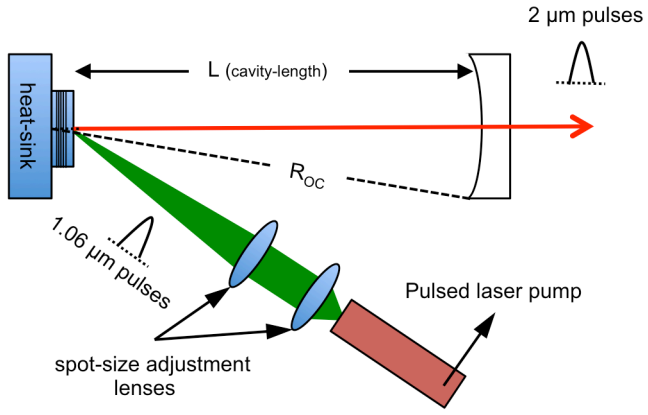

Figure 10: Schematic for optically pumped VECSEL operated in pulsed mode.

Figure 11 shows the pulsed peak output power versus peak pump power for a III-Sb VECSEL with AlGaAs/GaAs DBR. A linear cavity of length (**L_c** = 70 mm) is used for pulsed lasing of the devices. The output coupler has **R_{OC}** = **100mm** with Reflectivity, **R**~ 98%. The threshold incident pump power density is calculated to be 17.44 kW/cm^2. The peak output power from this device has been reported as high as 340 W [16].

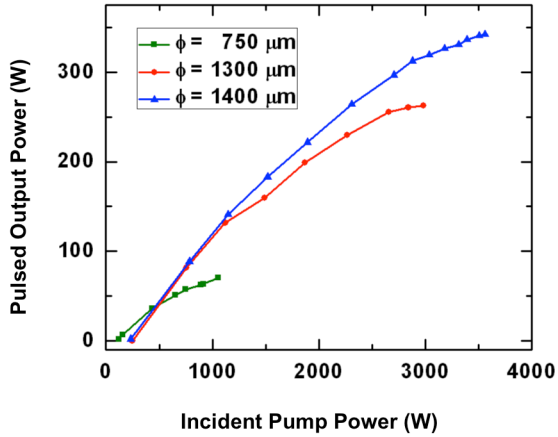

Figure 11: Peak output-power Vs peak pump power for the pulsed III-Sb VECSEL on GaAs substrate.

A. CW lasing characterization

The CW-lasing characterization setup is shown in Figure 12. The setup is significantly different for the CW pumping

compared to the pulsed pumping due to the fact that the CW setup will require the use of an intra-cavity heat-spreading element, which in this case is transparent diamond or silicon carbide (SiC). The process of fabricating the VECSEL with the epitaxially grown samples begins with the laser wafer thinned down from the substrate-side to ~ 100 µm; it is then soldered onto a heat sink using a thin Indium foil and or gold-metallization. In order to dissipate heat generated in active region, a transparent heat-spreader is attached to epi-side of the sample by means of capillary bonding.

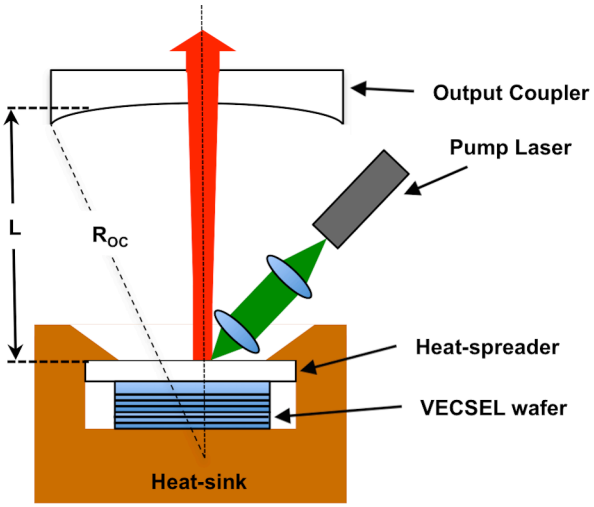

Figure 12: Schematic for optically pumped VECSEL operated in CW mode.

Figure 13 shows the L-L chracteristics for the VECSEL device grown on GaAs/AlGaAs DBR for heat-sink temperatures in range of -5 to 20 °C. A 980nm fiber coupled diode laser is used for photopumping of this VECSEL device. The device is pumped at an incident angle of 30° with a pump-spot size of 130 µm. SiC is used as an intracavity transparent heat spreader on the epi-surface. The threshold incident pump power density ($\mathbf{P_{th}}$) is calculated to be 13.9kW/cm^2 for laser operation at 20°C [17]. The maximum CW output power is observed to be ~ 120mW at a heat sink temperature of -5 °C. A similar setup is used for characterization of the latticematched III-Sb VECSEL.

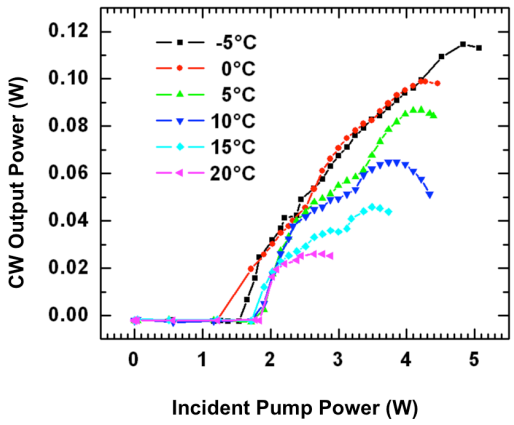

Figure 13: Output-power Vs Pump power for the CW III-Sb VECSEL on GaAs substrate.

IV. Discussions

A. Effect of mismatched epitaxy on VECSEL performance.

The mismatched III-Sb laser with GaAs/AlGaAs DBRs have a very similar structure to their lattice matched couterparts. However the performance of the antimonide VECSELs on GaAs is significantly poorer compared to the lattice-matched VECSELs on GaSb. This can be seen in table I which shows the key metrics for a latticemismached III-Sb VECSEL on GaAs/AlGaAs DBR versus those for a latticematched VECSEL grown on GaSb. The mismatched VECSEL's threshold pump power density is with 13.9 kW/cm^2 much higher than 1.19 kW/cm^2 for the latticematched VECSEL. Futhermore there is also a significant decrease in the wall-plug efficiency of the laser grown on GaAs and the maximum CW power achieved from such a laser. It can be speculated that the deterioration in the performance of the VECSEL when grown mismatched on GaAs compared to when it is grown lattice matched on GaSb can be attributed to the presence of threading dislocations in the active region when it is grown on GaAs/AlGaAs.

The carrier loss equation in VECSEL structures can be expressed as follows [18]

$$\mathbf{R_{loss} = R_{Defect} + R_{SE} + R_{Auger} + R_{remaining}} \quad (2)$$

where R_{loss} is the carrier loss equation rate, R_{Defect} is the carrier loss equation rate due to carrier recombination via defect states, R_{SE} is the loss due to spontaneous emission processes, R_{Auger} is the carrier loss due to Auger recombination processes and $R_{remaining}$ is the carrier loss due

to carriers not captured by wells or tunnelled carriers not re-captured in other wells. A widely accepted model to repesent such losses is also known as "ABC" model;

Table I: Performance comparison of lattice mismatched III-Sb VECSEL on GaAs/AlGaAs to lattice matched VECSEL on GaSb/AlAsSb.

TABLE I

Device	η_d	P_{th}	P_{Max} (CW)
VECSEL on GaAs/AlGaAs DBR	3.5 %	13.9kW/cm^2	120mW
VECSEL on GaSb/AlAsSb DBR	14.1%	1.19kW/cm^2	3W

$$R_{loss} = AN + BN^2 + CN^3 + R_{remaining} = N/\tau \qquad (3)$$

where τ is the carrier lifetime under low carrier concentration (no stimulated emission). In VECSEL structures typically $R_{remaining} \sim 0$, since most of the carriers generated in the barrier region are captured in the QWs with high probability and carrier capturing is also enhanced by the AlSb carrier confinement layers) . However the "ABC" empirical model is not adequate to model the carrier losses at high carrier density and high temperature (typical operating conditions of a high power VECSEL). A fully microscopic many-body approach used for computation of losses, has shown a better agreement between experimental and theoretical data [19,20] . Therefore, the carrier loss equations can be represented as follows;

$$R_{loss} = AN + R_{SE}(N,T) + R_{Auger}(N,T) = N/\tau \qquad (4)$$

Here R_{SE} and R_{Auger} are functions of carrier density and operating temperature of the device. One way to determine losses in the structure is by measuring the internal quantum efficiency. The internal quantum efficiency is defined as the ratio between carrier recombination rate through spontaneous emission to total number of absorbed pump photons: $\eta_i = R_{SE}/R_{loss}$. The defect recombination coefficient is estimated to be $A^{-1} = 2.6$ns for III-Sb VECSEL structures grown on GaAs/AlGaAs DBRs. The A^{-1} for the III-Sb VECSEL structure grown on GaSb substrates is determined to be 16ns. [14] The low value of A^{-1} for the VECSEL structure grown on GaAs substrates can be attributed to the presence of dislocations in the active region. These defects can act as non-radiative recombination centers. Thus the source of the threading dislocations and their density in the active region should be investigated.

B. TEM based analysis of threading dislocation density in the VECSELs.

The investigation of threading dislocation density in the III-Sb VECSELs involves the cross section transmission electron microscopy analysis of both the lattice mismatched and the lattice matched III-Sb VECSELs. These VECSELs are cross-sectioned with a focused ion beam (FIB) lift out using a FEI Helios 450 DIB system. The TEM imaging was completed using an FEI Tecnai F20 equipped with HAADF STEM detector. For the initial TEM/STEM imaging the samples were ~150nm near the top of the active region and ~250nm near the active/DBR interface.

The images of the lattice mismatched and the lattice matched antimonide VECSELs are shown in Figure 14. In case of the III-Sb VECSEL on GaAs/AlGaAs DBR, the strain from the lattice mismatch is to be relieved at the (GaSb/GaAs) interface through misfit-dislocations at interface [9]. However in many cases there are breaks and discontinuitites associated with the IMF interface which leads to threading dislocations at these points as can be seen in Figure 14 (a). Furhtermore these threading dislcoations are able to reach the quantum well active region and are the source for the non-radiative recombination in the lasers and the subsequenty reduced A^{-1} values. Figure 14 (b) shows the high resolution cross-sectional TEM image for the lattice matched VECSEL. This image shows the complete lack of threading disocations in the active region and is a significant improvement over the mismatched structure.

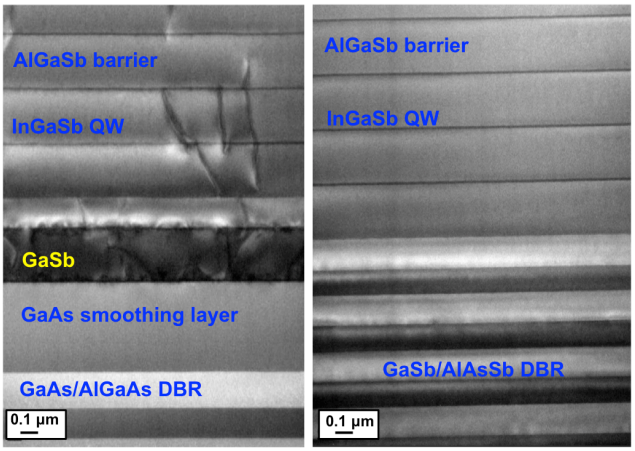

Figure 14: Transmission electron microscopy comparison of lattice mismatched III-Sb VECSEL on GaAs/AlGaAs to lattice matched VECSEL on GaSb/AlAsSb. Figure (a) shows the lattice mismatched structure with extensive threading dislcoations in the active region and (b) shows the complete absence of threading dislcoatinos in the lattice matched structure.

Thus from X-TEM image of the III-Sb VECSEL structure on GaAs/AlGaAs DBR it is evident that the dislocations are present in the active region. The presence of dislocations within diffusion length of carriers leads to a reduction in carrier lifetime. The carrier lifetime is related to dislocation density N_D by following formula, [21]

$$\frac{1}{\tau_d} = \frac{\pi^2 \mu k T N_D}{4q} \quad (5)$$

where τ_d is the carrier lifetime associated with recombination asssited by dislocations, μ is the mobility of carriers, q is the electronic charge. The overall carrier lifetime τ is then

$$\frac{1}{\tau} = \frac{1}{\tau_0} + \frac{1}{\tau_d} \quad (6)$$

where τ_0 is the carrier lifetime in dislocation free material. The carrier lifetime in the lattice matched III-Sb VECSEL is closer to τ_0 , as it is almost free of dislocations as can be seen in the high resolution TEM image. In a TEM image one can measure the total projected length in the TEM image plane of dislocation lines l'. The dislocation density can then be estimated using following formula [22],

$$N_D(cm^2) = \frac{4}{\pi}\frac{l'}{At} \quad (7)$$

where t is thickness of TEM sample , A is area over which the projected length l' is estimated. [23]

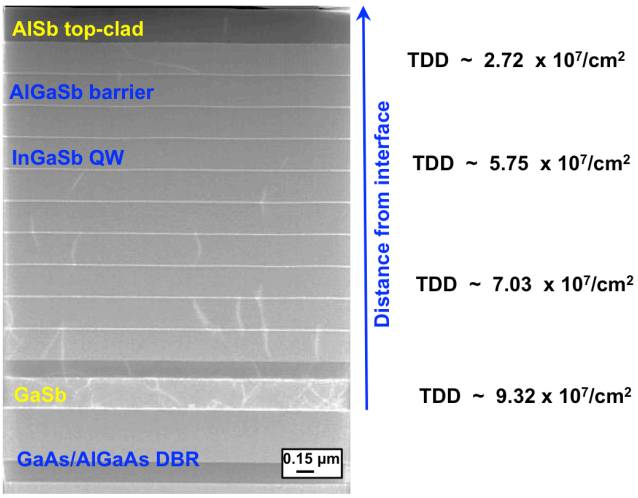

Figure 15: STEM image of lattice mismatched III-Sb VECSEL on GaAs/AlGaAs showing the source of the threading dislocations at the IMF array and subsequent reduction in the density as a function of distance from the mismatched interface.

In Figure 15 we estimate the dislocation density N_D as a function of distance from the GaSb/GaAs interface. The dislocation density reduces from ~ 10^8 cm^{-2} to about ~ 10^7 cm^{-2} at a distance of about ~ 3 μm from the interface. Thus it is evident from the relationship between carrier lifetime and dislocation density that the higher TDD found in the III-Sb on GaAs/AlGaAs DBRs is detrimental to performance of a VECSEL device. [14] Furthermore this high TDD in the III-Sb on GaAs/AlGaAs can also be linked to the high threshold density, lower efficiency and reduced maximum output power compared to a lattice matched III-Sb laser.

V. Threading Dislocation Reduction Strategies

The detrimental effect of the high TDD in the mismatched VECSEL's active region requires strategies for either reducing these dislocations or bending the dislocations before they can reach the active regions. One option is to improve the IMF layer when the GaSb is grown on GaAs and the second approach is to move the IMF further away from the active region.

A. Optimizing the IMF layer using Time-resolved photo-luminescence measurements.

The transmission electron microscopy analysis of the III-Sb active regions on GaAs/AlGaAs layer does provide proof about the existence of threading dislocations in the proximity of the quantum wells. However to optimize the IMF interface itself we require an alternate technique that can be used to characterize the interface in a more iterative and systematic manner. Time-resolved PL is used to investigate the effect of the IMF interface on optical properties of III-Sb active regions grown on GaAs. While we are yet to make use of this process to optimize quantum wells for the VECSEL active region, we have been able to demonstrate this approach to establish the effectiveness of the IMF interface on III-Sb active regions grown on GaAs substrates. For this purpose we have grown two QW samples on (001) GaAs substrates. Both samples have the same twin QW structures, i.e., 50-nm $Al_{0.5}Ga_{0.5}Sb$ barrier / 8-nm GaSb well / 50-nm $Al_{0.5}Ga_{0.5}Sb$ barrier / 8-nm GaSb well / 50-nm $Al_{0.5}Ga_{0.5}Sb$ barrier / 5-nm GaSb cap grown on 100-nm GaSb buffer layer. One sample was grown with the IMF at the GaSb/GaAs interface and the other without the IMF.

Time-resolved measurements were performed employing a Ti:Sapphire mode-locked laser generating 5-ps laser pulses tuned at 1.55 eV (800 nm) at the repetition rate of 76 MHz. The laser pulses were focused on the sample surface kept at 4 K in a liquid-He circulating cryostat via an objective lens with the numerical aperture of 0.42. Luminescence from the sample was collected with the same objective lens and was detected with a near-infrared streak camera (Hamamatsu C11293-01) combined with a 150-grooves/mm monochromator. The measurement time resolution was 20 ps.

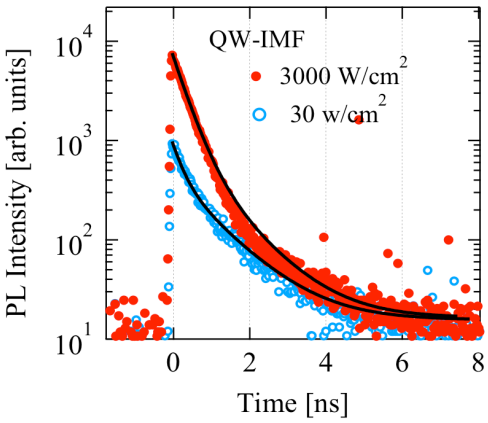

Figure (16) Transient PL decay measured on QWs grown with IMF with the average excitation powers of 30W/cm² and 3000W/cm².

The measured PL time decay was spectrally integrated at each transient time and the integrated intensities are shown in Fig. 16. The two sets of data are displayed for the average excitation power densities of 30 and 3000 W/cm^2. The measured transient PL intensities were generally well fitted with the double exponential function of $I(t)= I_{dark}+A_1\exp(-t/\tau_1)+ A_2\exp(-t/\tau_2)$, where I_{dark} is the dark counts without the pulsed laser excitation, A_1 and A_2 are the amplitudes of each term, and τ_1 and τ_2 are the decay time constants. These parameters were determined by the fittings shown by the solid lines in Fig. 16 and are summarized in Table II. To identify the origin of the two decay time constants of τ_1 and τ_2, we have studied the time decay by spectral integrations in limited ranges [23]. For example, the PL decay measured on the QW with IMF was spectrally separated into the two regions of 1367-1405 nm (882-907 meV) and 1406-1444 nm (859-882 meV) and integrated in each region. This spectral separation resulted in single exponential decays and the decay time constants determined in the lower and higher photon energy regions very nicely reproduced the τ_1 and τ_2 values given in Table II, respectively [23]. Therefore τ_1 and τ_2 are the decay time constants related to the QW ground states and the excited states, respectively.

Table II. Parameters determined from the fitting to the transient PL decay.

Excitation Power (W/cm²)	QW with IMF			QW without IMF		
	A_1/A_2	τ_1(ps)	τ_2(ps)	A_1/A_2	τ_1(ps)	τ_2(ps)
30	4.47	1006±21	222±6	6.78	1560±20	250±8
150	3.46	1000±14	260±7	6.44	1530±27	243±7
750	3.55	1050±17	310±7	6.23	1450±30	248±5
1550	2.98	1004±20	330±10	6.79	1550±26	258±7
3000	2.69	1019±28	351±8	6.58	1590±19	257±9

The comparison of the two sets of data in Table II on the QWs with and without IMF shows a clear difference of the excitation power dependence of the τ_2 value. With IMF the τ_2 value and the amplitude A_2 increased with the excitation power, while they were independent of the excitation power without IMF. After the pulsed laser excitation of the QW samples, the excited electrons and holes experience energy relaxation. Therefore the τ_2 value of the excited states includes this energy relaxation process and is much shorter than the τ_1 value of the ground states. The increase of the excitation power generally enhances the band filling of the QW ground states with the photo-generated carriers, and this reduces the energy relaxation rate in both the conduction and valence bands due to the filling of the energy states above the band edges. This will result in the increase of the τ_2 value for the QW with IMF. The enhanced steep decay in Fig. 16 for the higher excitation corresponds to the increase of the amplitude A_2. The fact that the QW without IMF did not show any excitation power dependence indicates the presence of residual defects that prevent the band filling effect in the QW ground states. The difference of the band filling effect is also clear from the measured PL spectra. The inset of Fig. 17 is the PL spectra measured with the CW excitation power of 2500 W/cm^2. The peak shift with the excitation power is plotted in Fig. 17. While the PL peaks in both QWs were observed at around 870 meV for the lower excitation power, the clear difference of the blue shift was observed at the higher excitations. The PL peak steadily blue shift for the QW with IMF with the band-filling effect, while the one without IMF showed much reduced blue-shift. This difference is consistent with the above discussions on the PL decay time constants. From the present PL measurements, we conclude that the QW with IMF exhibits superior optical properties with the reduction of the defects originating from the GaSb/GaAs highly mismatched hetero-interfaces.

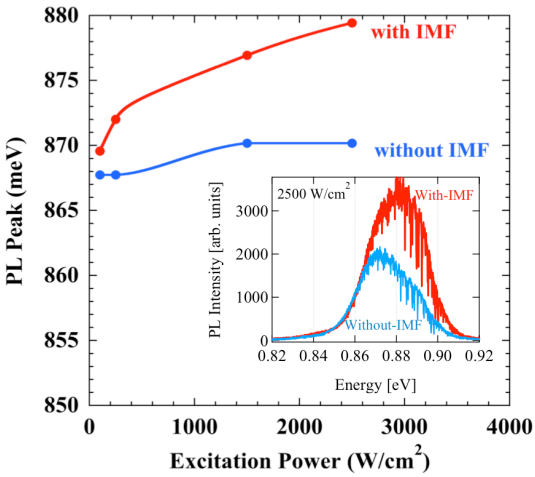

Figure (17) PL peak shift with the excitation power. Clear blue shift is observed with QW with IMF. Inset is the PL spectra measured at the excitation power of 2500 W/cm² on QWs grown with IMF and without IMF.

VI. Conclusions

We have demonstrated the growth and characterization of 2 μm III-Sb VECSELs on GaAs/AlGaAs DBRs with an active region consisting of nine InGaSb/AlGaSb quantum

wells. The VECSELs consist of an III-Sb active region with the lattice constant of GaSb (6.09 Å) and a GaAs/AlGaAs DBR with the lattice constant of GaAs (5.65 Å). The 7.78% mismatched is lattice constant is managed by establishing a 90^o array of misfit dislocations which ensures an ~100% relaxation of the GaSb layer and achieves a significant reduction in threading dislocation density. The lasers have been optimized for several parameters including the IMF interface, the quantum wells and the thickness of the individual layers. The III-Sb VECSELs on GaAs/AlGaAs DBRs were characterized for lasing performance under both sub-thermal pulsed conditions and continuous-wave conditions. The maximum output power obtained from mismatched VECSELs under pulsed and CW lasing conditions is 340W and 120mW respectively. The threshold pump density, efficiency and the maximum output power of the mismatched VECSELs were reduced compared to fully lattice matched III-Sb VECSELs. An analysis of the active region quality was conducted using transmission electron microscopy, which established the presence of extensive threading dislocations in the active region.

REFERENCES

[1] O.G. Okhotnikov, *Semiconductor Disk Lasers:Physics and Technology*. Weinheim, Germany: Wiley-VCH, 2010.

[2] B. Heinen et al., "106 W continuous-wave output power from vertical-external-cavity surface-emitting laser," *Electron. Lett.,* vol. 48, no. 9, pp. 516-517, Apr. 2012.

[3] M.Y.A. Raja, S.R.J. Brueck, M. Osinski, C.F. Schaus, and J.G. McInnerney, "Novel wavelength-resonant optoelectronic structure and its application to surface-emitting semiconductor lasers," *Electron. Lett.*, vol. 24, no. 18, pp. 1140–1142, Sept. 1988.

[4] A.C. Tropper and S. Hoogland, "Extended cavity surface-emitting semiconductor lasers," *Prog. Quantum Electron*., vol. 30, no. 1, pp. 1-43, Jan. 2006.

[5] A.M. Rocher, "Interfacial dislocations in the GaSb/GaAs (001) heterostructure," *Solid State Phenomena,* vols. 19-20, pp. 563-572, 1991.

[6] W. Qian, M. Skowronski, R. Kaspi, "Dislocation density reduction in GaSb films grown on GaAs substrates by molecular beam epitaxy," *J. Electrochem. Soc.,* vol. 144, no. 4, pp. 1430-1434, Jan. 1997.

[7] B. Brar, D. Leonard, "Spiral growth of GaSb on (001) GaAs using molecular beam epitaxy," *Appl. Phys. Lett.*, vol. 66, no. 4, pp. 463-465, Jan. 1995.

[8] B.R. Bennett, R. Magno, B.V. Shanabrook, "Molecular beam epitaxial growth of InSb, GaSb, and AlSb nanometer-scale dots on GaAs," *Appl. Phys. Lett.*, vol. 68, no. 4, pp. 505-507, Jan. 1996.

[9] S.H. Huang et al., "Strain relief by periodic misfit arrays for low defect density GaSb on GaAs," *Appl. Phys. Lett.*, vol. 88, pp. 131911-1 – 131911-3, Mar. 2006.

[10] A. Jallipalli, G. Balakrishnan, S.H. Huang, A. Khoshakhlagh, L.R. Dawson, D.L. Huffaker, "Atomistic modeling of strain distribution in self-assembled interfacial misfit dislocation (IMF) arrays in highly mismatched III-V semiconductor materials," *J. Cryst. Growth*, vol. 303, no. 2, pp. 449-455, May 2007.

[11] M.Mehta et al., "Room-temperature operation of buffer-free GaSb–AlGaSb quantum-well diode lasers grown on a GaAs platform emitting at 1.65 µm,"*IEEE Photon. Technol. Lett.*, vol. 20, no. 16, pp. 1628-1630, Oct. 2007.

[12] T. Yang, L. Lu, M. Shih, J. D. O'Brien, G. Balakrishnan, and D. L. Huffaker, "Room temperature InGaSb quantum well microcylinder lasers at 2 µm grown monolithically on a silicon substrate," *J. Vac. Sci. Technol.*, vol. 5, no. 5, pp. 1622-1625, Sept. 2007.

[13] A. Jallipalli, M.N. Kutty, G. Balakrishnan, J. Tatebayashi, N. Nuntawong, S.H. Huang, L.R. Dawson, D.L. Huffaker, Z. Mi, P. Bhattacharya, "1.54 µm GaSb/AlGaSb multi-quantum-well monolithic laser at 77 K grown on miscut Si substrate using interfacial misfit arrays," *Electron. Lett.*, vol. 43, no. 22, pp. 1198–1199, Oct. 2007.

[14] A. Laurain et al., "Influence of non-radiative carrier losses on pulsed and continuous VECSEL performance," in *Proc. Society of Photo-Optical Instrumentation Engineers (SPIE)*, 2012, vol. 8242, p. 82420S.

[15] A.R. Albrecht, "InAs quantum dot vertical-cavity lasers," Ph.D. dissertation, Dept. Phy. Astron., Univ. New Mexico, Albuquerque, 2009.

[16] Y.Y. Lai et al., "340-W peak power from a GaSb 2-µm Optically Pumped Semiconductor Laser (OPSL) grown mismatched on GaAs," *IEEE Photon. Technol. Lett.*, vol. 22, no. 16, pp. 1253-1255, Aug. 2010.

[17] T.J. Rotter et al., "Continuous-wave, room-temperature operation of 2-µm Sb-based optically-pumped vertical-external-cavity surface emitting laser monolithically grown on GaAs substrates," *Appl. Phys. Exp.*, vol. 2, pp. 112102-1—112102- 3, Nov. 2009.

[18] J. Hader, J.V. Moloney, S.W. Koch, L. Fan, M. Fallahi, "Carrier Recombination in Semiconductor Lasers: Beyond the ABC," *Numerical Simulation of Semiconductor Optoelectronic Devices, 2006. NUSOD '06. International Conference on,* pp. 39-40.

[19] J. Hader et al., "Predictive microscopic modeling of VECSELs," *IEEE J. Quantum Electron.*, vol. 46, no. 5, pp. 810–817, May 2010.

[20] J. Hader, J.V. Moloney, S. Koch, "Microscopic evaluation of spontaneous emission – and Auger – processes in semiconductor lasers," *IEEE J. Quantum Electron.*, vol. 41, no. 10, pp. 1217–1226, Oct. 2005

[21] J.E. Ayers, "Properties of semiconductors," in *Heteroepitaxy of Semiconductors: Theory, Growth, and Characterization*. Boca Raton, CRC Press, 2007, ch. 2, pp. 7-68.

[22] T.W. Butler, "On the determination of dislocation densities," USNA Engg. Dept., Annapolis, MD, Rep. E-69-1, May 1969.

[23] N.A. Jahan et al., "Spectral and transient luminescence measurements on GaSb/AlGaSb multiple quantum wells grown on GaSb/GaAs heterojunctions with and without interfacial misfit arrays," *Jpn. J. Appl. Phys.*, submitted for publication.

Pankaj Ahirwar is currently a PhD student in the Electrical and Computer Engineering department at The University of New Mexico. He received his undergraduate degree in Electrical Engineering from IIT Roorkee in 2005. His research interests include the epitaxial development and characterization of VECSELs based on antimonide active regions.

Thomas J. Rotter received the M.S. degree from the Westphaelische Wilhelms-Universitaet, Muenster, Germany, in physics in 1997, and the Ph.D. degree in Optical Sciences from the University of New Mexico (UNM), Albuquerque, USA, in 2007. From 2007 to 2009 he was a Research Scientist at the California NanoSystems Institute at UCLA, Los Angeles. In 2009 he joined the Center for High Technology Materials at UNM as a Research Assistant Professor. His current research interests include epitaxy and characterization of III-V arsenides, antimonides, and phosphides including highly mismatched materials and self assembled nanostructures for optical applications, in particular high power surface-emitting lasers. Thomas is a member of the Optical Society of America, the IEEE, and the Deutsche Physikalische Gesellschaft (German Physical Society).

Ganesh Balakrishnan is an Assistant Professor at the Center for High Technology Materials at the University of New Mexico. He received his B.E. in Electronics and Communications Engineering from the University of Madras, India in 2000. He received his M.S in Engineering with a specialization in communication engineering from the University of Toledo, OH in 2001. He obtained his PhD in Optical Sciences from the University of New Mexico in 2006. His research focus includes high-power vertical external-cavity surface-emitting laser development using quantum dot based and antimonide quantum well based active regions. He has co-authored 46 journal articles and over 50 conference presentations.